Available online at www.sciencedirect.com
SCIENCE DIRECT®
International Journal of Solids and Structures 42 (2005) 605–620
INTERNATIONAL JOURNAL OF SOLIDS and STRUCTURES
www.elsevier.com/locate/ijsolstr

On the fracture behavior of inhomogeneous materials—A case study for elastically inhomogeneous bimaterials

O. Kolednik [a,*], J. Predan [b], G.X. Shan [c], N.K. Simha [d], F.D. Fischer [e]

[a] *Erich Schmid Institute of Materials Science, Austrian Academy of Sciences, Jahnstrasse 12, A 8700 Leoben, Austria*
[b] *Faculty of Mechanical Engineering, University of Maribor, SI 2000 Maribor, Slovenia*
[c] *VOEST Alpine Industrieanlagenbau GmbH&Co, A 4031 Linz, Austria*
[d] *University of Miami, Coral Gables, FL 33124-0642, USA*
[e] *Institute of Mechanics, Montanuniversität Leoben and Erich Schmid Institute of Materials Science, Austrian Academy of Sciences, A 8700 Leoben, Austria*

Received 29 October 2003; received in revised form 31 January 2004
Available online 24 August 2004

Abstract

This paper presents a case study, examining the influence of a sharp bimaterial interface on the effective crack driving force in a fracture mechanics specimen. The inhomogeneity of the elastic modulus in linear elastic and non-hardening and hardening elastic–plastic bimaterials is considered. The interface is perpendicular to the crack plane. The material properties and the distance between the crack tip and the interface are systematically varied. The effect of the material inhomogeneity is captured in form of a quantity called "material inhomogeneity term", C_{inh}. This term can be evaluated either by a simple post-processing procedure, following a conventional finite element stress analysis, or by computing the J-integral along a contour around the interface, J_{int}. The effective crack driving force, J_{tip}, can be determined as the sum of C_{inh} and the nominally applied far-field crack driving force, J_{far}. The results show that C_{inh} can be accurately determined by both methods even in cases where J_{tip}-values are inaccurate. When a crack approaches a stiff/compliant interface, C_{inh} is positive and J_{tip} becomes larger than J_{far}. A compliant/stiff transition leads to a negative C_{inh}, and J_{tip} becomes smaller than J_{far}. The material inhomogeneity term, C_{inh}, can have the same order of magnitude as J_{far}. Based on the numerical results, the dependencies of C_{inh} on the material parameters and the geometry are derived. Simple expressions are obtained to estimate C_{inh}.

Keywords: Fracture toughness; Crack driving force; Inhomogeneous material; Interface; Material force; J-integral

* Corresponding author. Tel.: +43 3842 804 114; fax: +43 3842 804 116.
E-mail address: koledni k@unileoben.ac.at (O. Kolednik).

0020-7683/$ - see front matter © 2004 Elsevier Ltd. All rights reserved.
doi:10.1016/j.ijsolstr.2004.06.064

1. Introduction

Numerous researchers have demonstrated in theoretical and experimental studies that, if the material properties vary in the direction of the crack extension, the effective crack driving force (measured in terms of the stress intensity, K, or the near-tip J-integral, J_{tip}) becomes different from the nominally applied far-field crack driving force. Speaking in terms of the concept of material forces, the reason is that the material inhomogeneities induce an additional crack-driving force term, called the material inhomogeneity term, C_{inh}, which leads to a crack tip shielding or anti-shielding effect. The effective driving force, J_{tip}, is given by the sum of the nominally applied far-field crack driving force, J_{far}, and C_{inh}. This inhomogeneity effect is important for understanding the fracture behavior of all multiphase or composite materials, functionally gradient materials, as well as brazed or welded components and materials with special surface treatments, such as nitrided or case-hardened steels, or any coated material. The inhomogeneity effect offers also a promising basis for the design of materials and structural components where a variation of the material properties is intentionally introduced to increase the fracture resistance.

Experimental evidence that bimaterial interfaces influence crack growth can be found, e.g., in Suresh et al. (1992, 1993), Pippan et al. (2000). There exists a broad literature about the fracture mechanics of inhomogeneous materials. An extensive literature review is given in Simha et al. (2003) and shall not be repeated here. Very recent studies have been presented, e.g., by Jivkov and Ståhle (2003), Weichen (2003), Bahr et al. (2003), Kim and Paulino (2003), Rao and Rahman (2003), Wang et al. (2003), and Abendroth et al. (2002). Apart from the latter one, these recent papers deal with cracks in functionally graded materials. Classical fracture mechanics papers treat only elastic materials with restrictions regarding the geometry of the considered problem. Some numerical investigations have examined the effect of inhomogeneities in elastic–plastic materials. These studies show that J_{tip} is different from J_{far}, but the explanations are specific and cannot be easily extrapolated to general situations. Moreover, it has been noticed that it is a non-trivial task to accurately compute the crack-tip driving force J_{tip} when the crack tip comes close to an interface. It will be seen that our approach avoids these numerical complications as J_{tip} is determined from C_{inh} and J_{far}, and the latter values are easier to compute.

The concept of material forces, which is based on ideas by Eshelby (1970), is outlined in books by Maugin (1993), Gurtin (2000), and Kienzler and Herrmann (2000). The theory is appropriate for analyzing the behavior of all kinds of inhomogeneities in materials, such as point defects, dislocations, cracks, interfaces, phase boundaries, voids, or inclusions. The material forces approach has been used extensively to study fracture. Derivations of the crack driving force are found, e.g., in Gurtin and Podio-Guidugli (1996), Kienzler and Herrmann (2000), Simha (2000), and Steinmann (2000). The implementation into the finite element method has been demonstrated recently, e.g., in Steinmann et al. (2001), Kolling et al. (2002), Mueller and Maugin (2002), Mueller et al. (2002), and Denzer et al. (2003). However, only a few papers have examined the effect of inhomogeneous material properties on fracture. Honein and Herrmann (1997) used an invariant path-integral approach, but this derivation is restricted to a special distribution of inhomogeneities in elastic bodies. Maugin (1993) explores inhomogeneity effects in a general framework, but does not treat the effect of inhomogeneities on cracks.

In recently published papers, the material inhomogeneity term, C_{inh}, has been derived from the concept of material forces, first for a continuous variation of the material properties (Simha et al., 2003). Then, the theory has been extended to discrete jumps of the material properties at a sharp interface (Simha et al., submitted). The derivations do not require specific spatial distributions of the material inhomogeneities or specific constitutive relations of the materials. The material inhomogeneity term, C_{inh}, can be evaluated by a simple post-processing procedure, following a conventional finite element stress analysis. The ability of the procedure has been demonstrated in the above mentioned papers on a few selected examples. It has been shown that C_{inh} is positive and J_{tip} becomes larger than J_{far}, if a crack grows towards a more

compliant and/or lower strength material. A transition into a stiffer and/or higher strength material leads to a negative C_{inh}, and J_{tip} becomes smaller than J_{far}.

For both material scientists and engineers, it is important to predict for which material combinations the material inhomogeneity term has a large influence on the fracture behavior, for which it can be neglected, and which possibilities it offers for optimizing composite materials and structural components. Therefore, we want to present in this paper a comprehensive case study for a fracture mechanics specimen with a sharp bimaterial interface. The properties of the two materials and the distance between the crack tip and the interface are systematically varied, and C_{inh} and J_{tip} are evaluated for different values of J_{far}. The different influence factors on the material inhomogeneity term are worked out and, if possible, scaling relations are derived. Due to page limitations, we consider here only the effect of an inhomogeneity of the elastic modulus in both linear elastic and elastic–plastic bimaterials. The other cases, the effect of an inhomogeneity in the yield stress and in the strain hardening exponent, and the simultaneous variation of all the material parameters, will be treated in separate papers.

2. The crack driving force in bimaterial specimens

The relevant equations for evaluating the material inhomogeneity term have been derived in Simha et al. (2003, submitted), and the derivations shall not be repeated here. Only the relevant equations shall be given. Fig. 1 shows a two-dimensional body containing a crack and a sharp interface Σ. If the materials on the left and right of the interface are homogeneous and if there is a jump of the material properties at the interface, the material inhomogeneity term is given by

$$C_{\text{inh}} = -\mathbf{e} \cdot \int_{\Sigma} ([[\phi]]\mathbf{I} - \langle \boldsymbol{\sigma} \rangle \cdot [[\text{grad}\,\mathbf{u}]]) \cdot \mathbf{n}\,\mathrm{d}s. \tag{1}$$

$\boldsymbol{\sigma}$ is the Cauchy stress, $\mathbf{u}$ the displacement, $\mathbf{I}$ the identity matrix, $\mathbf{e}$ the unit vector in the direction of crack growth, and $\mathbf{n}$ the unit normal to the interface Σ. The stored elastic energy density, ϕ, is a function of the

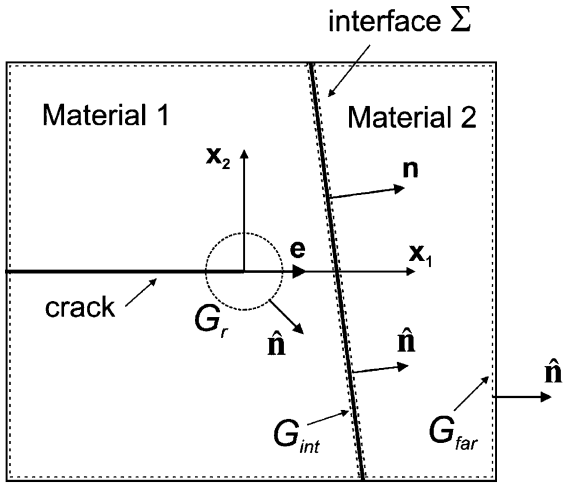

Fig. 1. A bimaterial body containing a crack and a sharp interface. The materials left and right of the interface are homogeneous and there is a jump of the material properties at the interface. $\mathbf{e}$ is the unit vector in the direction of crack growth, $\mathbf{n}$ the unit normal to the interface, and $\hat{\mathbf{n}}$ is the outer unit normal to the contours G_r, G_{int}, and G_{far} where the J-integral is evaluated.

linear strain tensor, $\boldsymbol{\varepsilon} = (\operatorname{grad}\mathbf{u} + \operatorname{grad}\mathbf{u}^{\mathrm{T}})/2$. In Eq. (1), the jump in a quantity $\mathbf{a}$ at the interface is designated as $[[\mathbf{a}]] = (\mathbf{a}^{+} - \mathbf{a}^{-})$, and $\langle\mathbf{a}\rangle = (\mathbf{a}^{+} + \mathbf{a}^{-})/2$ is the average across the interface, where $\mathbf{a}^{+}$ and $\mathbf{a}^{-}$ denote the limiting values of the quantity on either side of the interface. Note that the unit normal $\mathbf{n}$ points from the "–" to the "+" side. The tractions and displacements are continuous at the interface; the strain does not need to be continuous and is restricted by the Hadamard compatibility conditions (see Simha et al., submitted).

To compute the material inhomogeneity term, Eq. (1) has been transformed to (Simha et al., submitted)

$$C_{\mathrm{inh}} = -\int_{\Sigma} ([[\phi]] - \langle\sigma_{ik}\rangle[[\varepsilon_{ik}]])n_j e_j \,\mathrm{d}s. \tag{2}$$

If there is no sharp interface in the body, but instead a continuous variation of the material properties, the material inhomogeneity term becomes, with $\mathbf{x}$ being the position vector in the reference coordinate,

$$C_{\mathrm{inh}} = -\mathbf{e}\cdot\int_{D} \frac{\partial\phi(\boldsymbol{\varepsilon},\mathbf{x})}{\partial\mathbf{x}}\,\mathrm{d}A. \tag{3}$$

In Eq. (3), D is the region between the contour around the crack tip, G_r, and the external boundary of the body, G_{far}. Note that, when applying Eq. (3), the elastic energy density ϕ does not only depend on the local strain but also explicitly on $\mathbf{x}$. To make this clear, consider an elastic body with a crack as depicted in Fig. 1, but with the sharp interface replaced by a gradient layer between Material 1 and Material 2. Let the elastic modulus be a smooth function of the reference coordinate within the layer, $E = E(\boldsymbol{x})$, but constant left and right of the layer, $E = E_1$ and $E = E_2$, respectively. All other material properties shall be constant throughout the whole body. Although the strain field $\boldsymbol{\varepsilon}$ varies (with $\mathbf{x}$) throughout the whole body, a contribution to the material inhomogeneity term arises only in the interlayer where $\frac{\partial\phi}{\partial\mathbf{x}} = \frac{\partial\phi}{\partial E}\frac{\partial E}{\partial\mathbf{x}}$ is non-zero.

In the equations above, the integral in the right-hand side is a vector representing the total material force induced by the sharp interface (Eq. (1)) or the continuous variation of the material properties in the volume D (Eq. (3)). The scalar quantity C_{inh} is the projection of this vector in the direction of the crack growth, $\mathbf{e}$, and give the energy that is released during a unit crack extension due to these material inhomogeneities.

By definition, the effective, near-tip crack driving force, J_{tip}, can be evaluated as (Simha et al., 2003)

$$J_{\mathrm{tip}} = \mathbf{e}\cdot\lim_{r\to 0}\int_{G_r}\left(\phi\mathbf{I} - \operatorname{grad}\mathbf{u}^{\mathrm{T}}\boldsymbol{\sigma}\right)\cdot\hat{\mathbf{n}}\,\mathrm{d}s, \tag{4}$$

which is identical to the J-integral of fracture mechanics (e.g., Rice, 1968). In Eq. (4), G_r is a circle of radius r, centered at the crack tip, and $\hat{\mathbf{n}}$ is the outer normal to the contour G_r.

When material inhomogeneities are present, the effective crack driving force is given by

$$J_{\mathrm{tip}} = J_{\mathrm{far}} + C_{\mathrm{inh}}, \tag{5}$$

where J_{far} is the J-integral along the external boundary of the body, G_{far}. For a body with homogeneous material properties, $C_{\mathrm{inh}} = 0$ and J is path independent. If the material is inhomogeneous, but the material properties do not vary in the direction of crack extension, e.g., the body has an interface parallel to the crack, the integrals in Eq. (1) or (3) have a non-zero component only perpendicular to the unit vector in the direction of crack growth, $\mathbf{e}$. Thus, $C_{\mathrm{inh}} = 0$ and J is again path independent, compare also Eq. (2).

After a conventional finite element stress analysis, the material inhomogeneity term, C_{inh}, can be evaluated from Eq. (2). It has been demonstrated in Simha et al. (submitted) that for a sharp interface, there is an alternative method to compute the material inhomogeneity term by evaluating the J-integral along a contour G_{int} around and close to the interface,

$$J_{\mathrm{int}} = \mathbf{e}\cdot\int_{G_{\mathrm{int}}}\left(\phi\mathbf{I} - \operatorname{grad}\mathbf{u}^{\mathrm{T}}\boldsymbol{\sigma}\right)\cdot\hat{\mathbf{n}}\,\mathrm{d}s. \tag{6}$$

It can be shown that

$$C_{\text{inh}} = -J_{\text{int}}. \tag{7}$$

Finally, it should be noted that the integral, Eq. (6), can be also deduced from the standard J-integral concept, e.g., by extending the integration path G_{far} in Fig. 1 upwards and downwards along the interface. If no singularities occur at the points where the interface intersects the free surface, the J-integral splits into two terms. The first term is J_{far}, the second one is $-J_{\text{int}}$ (see Kichuchi and Miyamoto, 1984). As outlined in Simha et al. (submitted), the material forces concept, which has the advantage that it is a general concept which is free from any restricting assumptions on the material behavior, leads to the well known special solution reported above.

In the following, a case study is presented where the above equations are applied.

3. Numerical realization

We consider a compact tension (CT-) specimen (according to the ASTM or ESIS standards) made of two homogeneous isotropic materials, separated by a sharp interface. The specimen width is $W = 50$ mm, the height from the crack plane to the upper or lower surface is $h = 30$ mm, and the crack length $a = 29$ mm. The sharp interface is perpendicular to the crack plane, a distance L in front of the crack tip. For modeling the effect of different distances between crack tip and interface, the crack length is kept constant and the position of the interface in the specimen is varied.

We use the finite element (FEM) program (ABAQUS, http//www.hks.com) to perform the stress analysis. Fig. 2 shows the mesh of the specimen. The minimum mesh dimension is 0.013 mm at the crack tip and 0.05 mm at interface.

Isotropic, linear elastic or elastic–plastic materials are assumed to be perfectly bonded at the interface. Elastic–plastic materials are modeled using the incremental plasticity model provided by ABAQUS. The computations are performed under plane strain conditions. It is assumed that the problems investigated can be analyzed accurately enough by using the small strain formulations. The loading is controlled by prescribing the load-line displacement. Once the equilibrium stress and strain fields are known for each

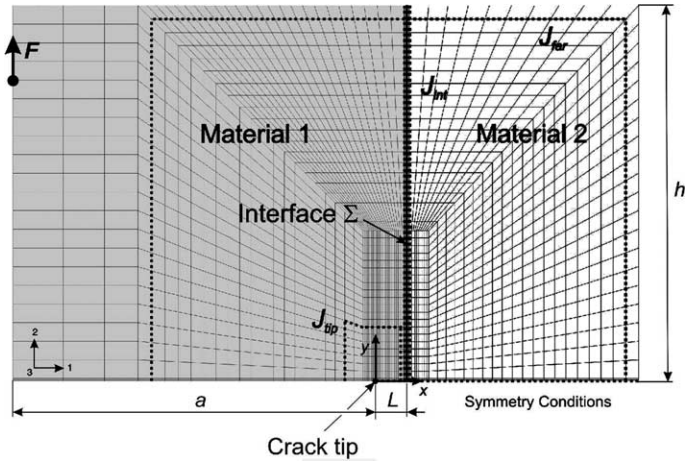

Fig. 2. Finite-element mesh of the CT-specimen with a bimaterial interface perpendicular to the crack. The paths for evaluating the J-integrals around the crack tip and the interface, as well as the far-field J-integral are indicated.

increment of displacement, the material inhomogeneity term, C_{inh}, the values of the J-integrals, J_{tip} and J_{far}, and the J-integral around the interface, J_{int}, will be calculated independently to check whether Eqs. (5) and (7) are fulfilled.

To compute the material inhomogeneity term according to Eq. (2), the values of the stress and strain components can be taken either directly from the integration points of the elements, or from extrapolated values at the nodes of the elements on both sides of the interface. The integration along the interface can be performed by the numerical integration method (in the case where the values at the integration points are used), or by simply using the trapezoid formula. For this paper, the extrapolated values and the trapezoid formula are used. In order to get sufficient accuracy, the FEM mesh must be fine enough around the crack tip and along the whole interface. Test calculations have shown that higher order elements, e.g., two-dimensional 8-node elements, give much better results than the first order elements. Hence, higher order elements are used.

The values of the J-integral are evaluated using the virtual crack extension method of ABAQUS. A rectangular contour near the outer specimen boundary is used for the evaluation of J_{far}. To test the procedure, the J-integral was calculated for a series of contours around the crack tip. Special crack tip elements were tested to model the different singularities for, e.g., the linear elastic and ideally plastic cases. Although the FEM solutions did not coincide in the elements directly adjacent to the crack tip, the J-values had only small variations, if the contours were a few elements away from the tip (and did not cross the interface). Hence, such a contour is used to calculate J_{tip}. Nevertheless, as will be seen below, J_{tip} can become inaccurate for small L and high loading.

The J-integral around the interface, J_{int}, is also evaluated using the virtual crack extension method of ABAQUS. This is done by specifying the set of nodes on the interface as virtual crack tip nodes. Even a contour directly adjacent to the interface yields very accurate results. For the evaluation of the J-integral, the virtual crack growth direction must be specified; it is the $(1,0)$-direction (see Fig. 2). If the same virtual growth direction is taken also for the interface, we get $J_{int} = -C_{inh}$ as in Eq. (7); if the $(-1,0)$-direction were taken, J_{int} would have the same value but the opposite sign.

Thus, we can get three independent values of the material inhomogeneity term, C_{inh}: (1) directly from Eq. (2), (2) from the J-integral around the interface, J_{int}, and Eq. (7), (3) from the difference between the near-tip and the far-field J-integral, Eq. (5). These values can be used to assess the accuracy of the computations.

4. A case study: Compact tension specimen containing a bimaterial interface

4.1. Linear elastic materials

First, we consider bimaterial specimens consisting of two linear elastic materials with different elastic modulus. The Poisson's ratio is taken as $\nu = 0.3$ for both materials. The computations are performed for a stationary crack, but the distance between crack tip and interface is varied, $-2.5\ \text{mm} \leqslant L \leqslant 2.5\ \text{mm}$.

In Fig. 3, the results are presented for two materials with a Young's modulus of $E = 70$ GPa (corresponding to aluminum) and 210 GPa (corresponding to steel) and a distance between crack tip and interface, $L = 1.25$ mm. The material inhomogeneity term, C_{inh}, the J-integral around the interface, J_{int}, and the difference of the near-tip and the far-field J-integrals, $J_{tip} - J_{far}$, are plotted vs. the nominally applied far-field crack driving force, J_{far}. Two cases are presented: The upper curves belong to the case where steel is Material 1, to the left of the interface with the crack mouth in it (compare Fig. 2), and aluminum is Material 2, on the right-hand side. We call this case "stiff/compliant transition". C_{inh} is positive and enhances the effective near-tip crack driving force, J_{tip} (see Eq. (5)). The lower curves in Fig. 3 belong to the case where aluminum is on the left-hand side and steel on the right-hand side (compliant/stiff transition). Here, C_{inh} is

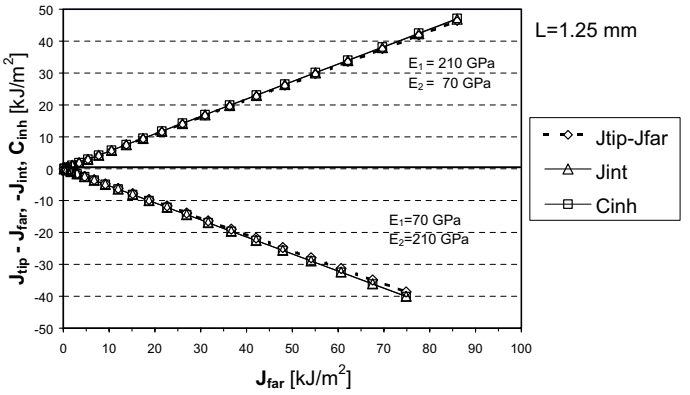

Fig. 3. Material inhomogeneity term, C_{inh}, J-integral around the interface, $-J_{int}$, and the difference of the near-tip and the far-field J-integral, $J_{tip} - J_{far}$, for a linear elastic bimaterial specimen. Upper curves: stiff/compliant transition, lower curves: compliant/stiff transition. L is the distance between crack tip and interface.

negative and diminishes J_{tip}. In both cases, the absolute size of the material inhomogeneity term, $|C_{inh}|$, increases linearly with J_{far}. This is expected for purely elastic materials as, according to the K-field solution, the elastic strain energy density is proportional to J_{far}. A closer look reveals that the absolute sizes of C_{inh} are similar, but not equal for the two cases, stiff/compliant and compliant/stiff transition. It is further seen from Fig. 3 that C_{inh} coincides with both J_{int} and $J_{tip} - J_{far}$, as it should be according to Eqs. (5) and (7).

In Simha et al. (2003), a 0.5 mm thick layer with a linear variation of the Young's modulus between Material 1 and Material 2 was considered. The distance between crack tip and the midsection of the layer was 1.25 mm. A comparison to the solution of a sharp interface resulted coinciding C_{inh} vs. J_{far} curves (Simha et al., 2002). It should be noted that, due to difficulties in the numerical evaluation, plane stress conditions were assumed in both studies. Compared to the results of these studies, the absolute values of the slopes of the C_{inh} vs. J_{far} curves for plane strain conditions, Fig. 3, are 2% and 4% lower for the stiff/compliant and compliant/stiff transition, respectively.

Fig. 4 shows a similar diagram for $L = 0.15$ mm, but more curves are included. It is seen that those curves coincide where the ratio of the Young's modulus, $M = E_1/E_2$, is identical, e.g., the curve for $E_1 = 630$ GPa and $E_2 = 210$ GPa coincides with the curve for $E_1 = 210$ GPa and $E_2 = 70$ GPa. In spite of the small distance between crack tip and interface, the C_{inh}-values come again close to both the J_{int}- and the $(J_{tip} - J_{far})$-values, even for high values of J_{far}. The curves are clearly non-symmetric with respect to the line $C_{inh} = 0$; the stiff/compliant transition produces larger $|C_{inh}|$-values than the compliant/stiff transition. The reason is that for the compliant/stiff transition, C_{inh} is negative and reduces J_{tip}, Eq. (5). As the effective crack driving force cannot become negative, $C_{inh} \geqslant -J_{far}$ so that $J_{tip} \geqslant 0$. The limiting line $C_{inh} = -J_{far}$ (for $M \to 0$) is also indicated in Fig. 4. For the stiff/compliant transition, the slope of the C_{inh} vs. J_{far} curve becomes infinite for $M \to \infty$. The small insertion in Fig. 4 depicts the C_{inh}-, J_{int}-, and the $(J_{tip} - J_{far})$-curves for $M = 10^4$ and $M = 10^{-4}$. The lower curve, for $E_1 = 21$ MPa, $E_2 = 210$ GPa, fits well to the limiting curve, $C_{inh} = -J_{far}$.

Similar computations are repeated for negative L, i.e., when the crack has penetrated through the interface so that the crack tip is actually in Material 2. Fig. 5 collects all data: The slope of the C_{inh} vs. J_{far} curve, $k = C_{inh}/J_{far}$, is plotted against L for different Young's modulus ratios M. Note that from Eq. (5), the effective, near-tip crack driving force becomes $J_{tip} = J_{far}(1 + k)$. Thus, Fig. 5 shows the relative change of the effective crack driving force due to the elastic modulus inhomogeneity, compared to a homogeneous material which is loaded to the same J_{far}. For example, the crack driving force is increased by 63% for a Young's modulus ratio $M = 2$ and $L = 0.3$ mm. The curves shows that $|k|$ increases when the distance between the

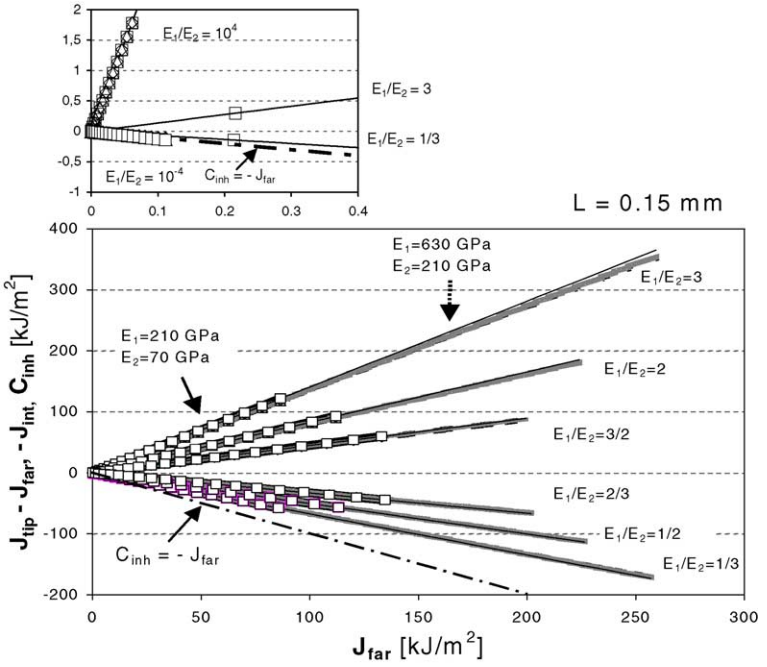

Fig. 4. Material inhomogeneity term, C_{inh}, J-integral around the interface, $-J_{\text{int}}$, and the difference of the near-tip and the far-field J-integral, $J_{\text{tip}} - J_{\text{far}}$, for a linear elastic bimaterial specimen. The curves coincide when the ratio of the Young's modulus, $M = E_1/E_2$, is constant. The small figure above shows the curves for $M = 10^4$ and $M = 10^{-4}$. The line, $C_{\text{inh}} = -J_{\text{far}}$, is the limiting curve for the compliant/stiff transition when the Young's modulus ratio, $M \to 0$.

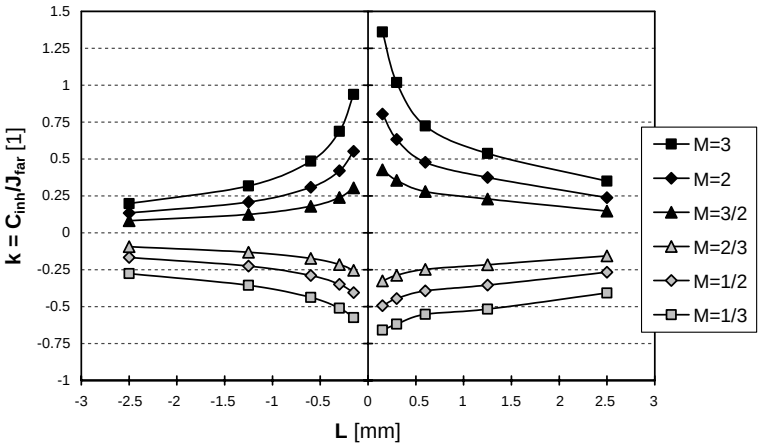

Fig. 5. The ratio of the material inhomogeneity term vs. the far-field J-integral plotted against the distance between crack tip and interface, L, for a linear elastic bimaterial specimen with different Young's modulus ratios M.

crack tip and the interface, L, decreases, but the curves are not symmetric with respect to the line $k = 0$. If the crack tip approaches the interface, $L \to 0$, the slope k approaches infinity for the stiff/compliant transitions, but k approaches -1 for the compliant/stiff transitions. It is also seen that the curves are not

symmetric with respect to the line $L = 0$: For the same distance to the crack tip, the interface induces smaller values of $|C_{inh}|$ for $L < 0$ than for $L > 0$.

In Simha et al. (2003), an estimate has been presented:

$$k = \frac{C_{inh}}{J_{far}} = \frac{1}{4\pi(1-\nu)} \frac{E_1 - E_2}{E_1 + E_2} \Psi, \tag{8}$$

with

$$\Psi = (3-4\nu) \ln \left(\frac{\sqrt{h^2 + L^2} + h}{\sqrt{h^2 + L^2} - h} \right) + 4(1-2\nu) \arctan \left(\frac{h}{L} \right) - \frac{2h}{\sqrt{h^2 + L^2}}. \tag{9}$$

In Eq. (9), h is half of the height of the specimen, or the maximum distance between a point along the interface and the crack plane. (Remember, for our specimen geometry, $h = 30$ mm.) The following simplifying assumptions were adopted in this estimate:

1. The stresses were taken from the K-field solution of homogeneous materials. Thus, the sharp interface and inhomogeneous material properties were ignored.
2. For calculating the stresses at the sharp interface, the elastic modulus was taken to be the average $(E_1 + E_2)/2$.

Due to these assumptions, Ψ cannot be accurate, and the estimated C_{inh}-values are too high, e.g., by a factor ~0.665 for $L = 1.25$ mm. Taking this factor into account, Eq. (8) tends to overestimate C_{inh} compared to the FEM result for the stiff/compliant transitions and to underestimate C_{inh} for the compliant/stiff transitions when $L \to 0$. The reason is that Ψ approaches infinity for $L \to 0$, and Eq. (8) yields k–L curves which are symmetric with respect to the line $k = 0$. Nevertheless, Eq. (8) demonstrates that for linear elastic bimaterials, the material inhomogeneity term is proportional to J_{far} and the relative jump of the Young's modulus at the interface. Note that the term $(E_1 - E_2)/(E_1 + E_2) = (M - 1)/(M + 1)$ is identical to the first Dundurs parameter (Dundurs, 1969) for plane strain conditions and constant Poisson's ratio.

4.2. Elastic–plastic materials

Next, we consider bimaterial specimens consisting of two linearly elastic-ideally plastic materials. The two materials shall have the same yield stress but different elastic modulus. In both materials, the Poisson's ratio is set to $\nu = 0.3$ for the elastic regime and $\nu = 0.5$ for the plastic regime. The stress and strain analysis is performed using the incremental plasticity model provided by ABAQUS. It should be noted, however, that for calculating C_{inh} by Eq. (2), ϕ is taken as the total strain energy density and ε_{ik} as the components of the total strain. Thus, in the post-processing procedure, the material is treated as if it were non-linear elastic.

Fig. 6 compares C_{inh} to J_{int} and $(J_{tip} - J_{far})$ for $L = 1.25$ mm and a yield stress of $\sigma_y = 500$ MPa (and a strain hardening exponent $N = 0$ as the material is non-hardening). C_{inh} coincides with J_{int} even at very large values of J_{far}, but $(J_{tip} - J_{far})$ coincides only for small J_{far}-values. The deviation starts between $J_{far} \geqslant 80$ kJ/m^2 (for $E_1 = 210$, $E_2 = 140$ GPa) and is caused by the relatively low accuracy in the calculation of J_{tip}. For smaller L, the deviation starts even earlier, e.g., at $J_{far} \geqslant 15$ kJ/m^2 (for $L = 0.15$). It will be seen in the next section that the error in J_{tip} is not caused due to the non-hardening material (see Fig. 11). C_{inh} and J_{int} always show a good coincidence; e.g., for $L = -0.15$ mm and $\sigma_y = 900$ MPa, which is the worst case, the maximum deviation is 3%.

For small values of J_{far}, the slopes of the C_{inh} vs. J_{far} curves come close to those of the corresponding linear elastic case (compare Fig. 6 and Fig. 3). We call these parts of the curves "quasi-linear parts",

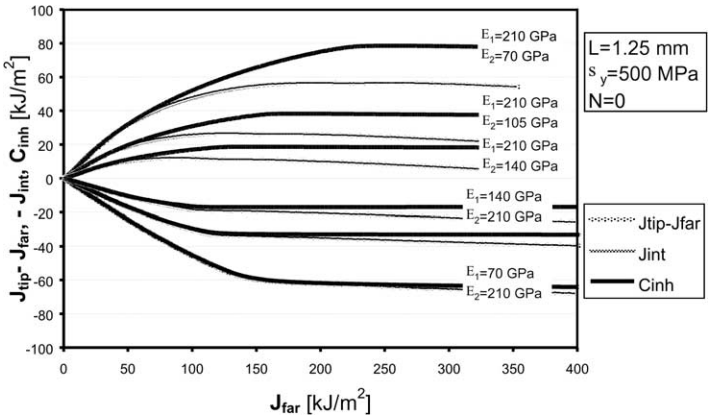

Fig. 6. Material inhomogeneity term, C_{inh}, J-integral around the interface, $-J_{int}$, and the difference of the near-tip and the far-field J-integral, $J_{tip} - J_{far}$, for an elastic-ideally plastic bimaterial specimen with constant yield stress and an inhomogeneity in the Young' modulus. The C_{inh} vs. J_{far} curves approach a saturation value at high J_{far}.

although a closer look reveals that the curves are not linear but have rather a sigmoidal shape. The curves for the stiff/compliant transition are steeper, the curves for the compliant/stiff transition are flatter, compared to the linear elastic case. With increasing J_{far}, the C_{inh} vs. J_{far} curves become flatter and flatter and approach a saturation value, $\hat{C}_{inh}$, at high J_{far}. The $\hat{C}_{inh}$-values differ strongly for the different Young's modulus ratios and are not fully symmetric regarding the line $C_{inh} = 0$.

Curves similar to Fig. 6, but for plane stress conditions, have been published in Simha et al. (2003) for a 0.5 mm thick graded layer and in Simha et al. (2002) for a sharp interface. The graded layer produced slightly ($\sim$10%) lower C_{inh}-values than the sharp interface. It should be noted that Kim et al. (1997) compared the material inhomogeneity effect in a bimaterial with constant elastic modulus but different yield stresses to those in a bimaterials with a graded interlayer. The comparison has been made by computing the near-tip J-integral, J_{tip}, for given far-field values, J_{far}. The computations were made for plane stress conditions. Only small differences have been found between the graded and the sharp transition. Contrary to the linear elastic case, here a big difference between plane stress and plane strain conditions appears: for plane strain conditions, the saturation value of the material inhomogeneity term, $\hat{C}_{inh}$, is much higher (by nearly a factor 3) and the saturation value is reached at a much higher J_{far}.

Fig. 7 shows the effect of different yield stresses for $L = 0.60$ mm. It is seen that the saturation value, $\hat{C}_{inh}$, depends strongly on the yield stress. It is clear that the inhomogeneity effect saturates when the plastic zone has reached its maximum size and the specimen has reached the limit load. For materials with a lower yield stress, the saturation is reached earlier, and the saturation value, $\hat{C}_{inh}$, is smaller than for the materials with a higher yield stress. Saturation is reached earlier (i.e., at lower J_{far}-values) and the $\hat{C}_{inh}$-values are smaller for the compliant/stiff transition than for the stiff/compliant transition.

Curves similar to those of Figs. 6 and 7 are generated for all other L-values between -2.5 mm $\leqslant L \leqslant 2.5$ mm but are not presented here. Instead, Fig. 8 presents an overview of the size of the material inhomogeneity term for a Young's modulus of 210 and 70 GPa, respectively, and a yield stress of $\sigma_y = 500$ MPa. For different values of J_{far} between 40 and 240 kJ/m^2, C_{inh} is plotted against the distance between the crack tip and the interface, L. When a crack approaches the interface to a more compliant material (at constant J_{far}), C_{inh} first increases with decreasing L, reaches a maximum value at a distance between $L = 0.6$ mm (for $J_{far} = 40$ kJ/m^2) and $L = 1.3$ mm (for $J_{far} = 240$ kJ/m^2), and then decreases. When the crack has penetrated the interface, the decrease of C_{inh} slows down and the inhomogeneity effect seems to approach an asymptotic value. The strong non-symmetry with respect to the line $L = 0$ occurs because of the forward

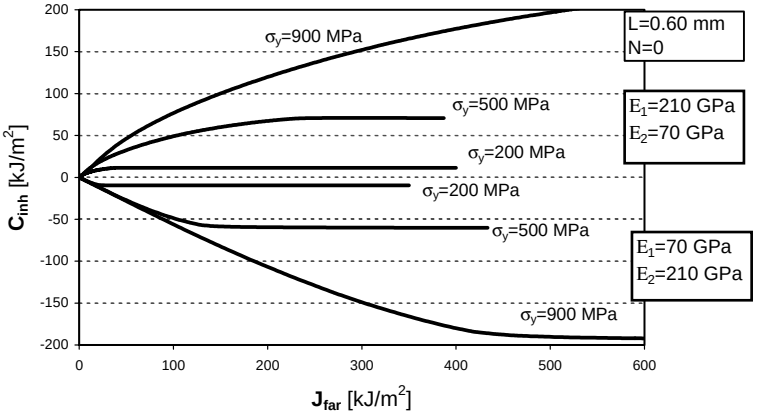

Fig. 7. The effect of the yield stress on the material inhomogeneity term, C_{inh}, for an elastic-ideally plastic bimaterial specimen with constant yield stress and an inhomogeneity in the Young' modulus.

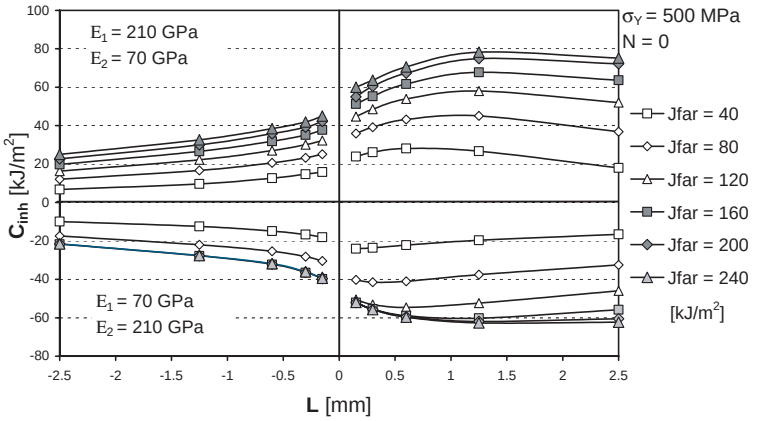

Fig. 8. The size of the material inhomogeneity term, C_{inh}, plotted against the distance between crack tip and interface, L, for different values of J_{far}. C_{inh} reaches its maximum value at a distance between $L = 0.6$ mm (for $J_{\text{far}} = 40$ kJ/m^2) and $L = 1.3$ mm (for $J_{\text{far}} = 240$ kJ/m^2). At $J_{\text{far}} = 240$ kJ/m^2, C_{inh} has reached everywhere its saturation value, $\hat{C}_{\text{inh}}$.

orientation of the plastic zone, i.e., the plastic zone is not circular and centered to the crack tip but has its maximum extension at a certain angle ($\theta \approx 70°$ for a homogeneous material) with respect to the crack plane. Again, it is seen that the C_{inh} vs. L curves are not fully symmetric with respect to the line $C_{\text{inh}} = 0$. It should be also noted that at a loading of $J_{\text{far}} = 240$ kJ/m^2, the material gradient term has reached its saturation value, $\hat{C}_{\text{inh}}$, for all values of L. Thus, the maximum $\hat{C}_{\text{inh}}$-values for this material combination and geometry are 78 kJ/m^2 for the stiff/compliant transition and 63 kJ/m^2 for the compliant/stiff transition.

Fig. 9 shows the deformation of the bimaterial specimen with $E_1 = 210$, $E_2 = 70$ GPa, $\sigma_y = 500$ MPa, $L = 1.25$ mm for a loading corresponding to $J_{\text{far}} = 237$ and 350 kJ/m^2, respectively. At both J_{far}-values, the saturation value, $\hat{C}_{\text{inh}}$, has been reached and the C_{inh} vs. J_{far} curve is horizontal, see Fig. 6. The iso-lines in Fig. 9 indicate the equivalent plastic strain. It is seen that the shape of the plastic zone remains unchanged at the interface; it changes only in Material 2.

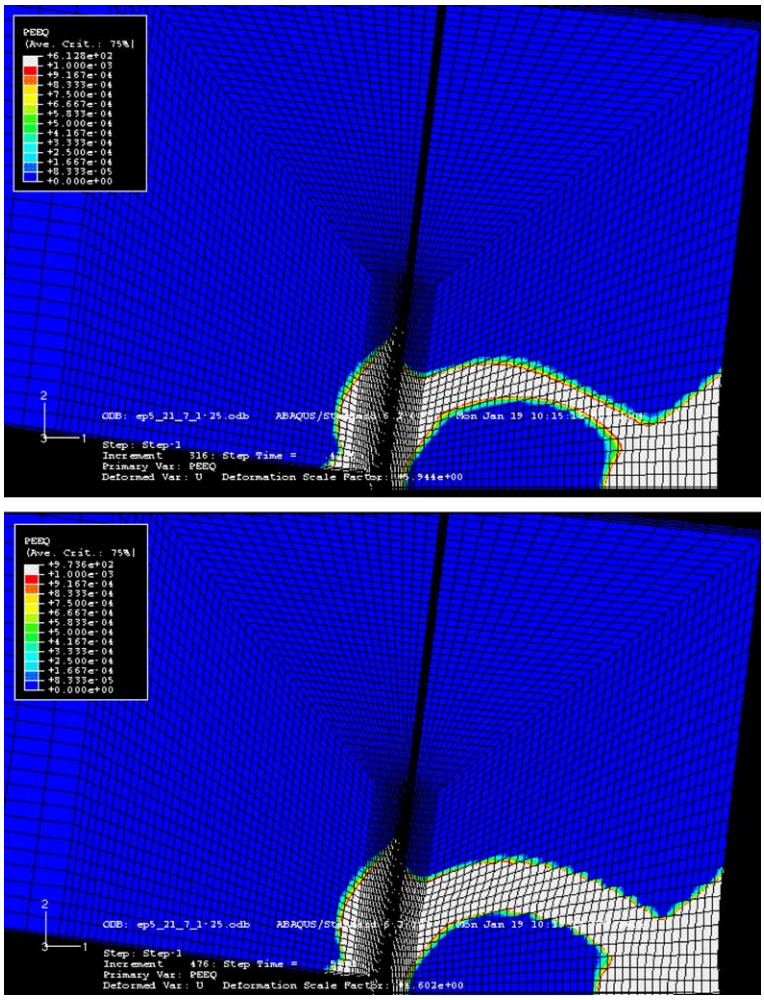

Fig. 9. The shape of the plastic zone at $J_{far} = 237$ kJ/m^2 and $J_{far} = 350$ kJ/m^2 for a bimaterial specimen with $E = 210/70$ GPa, $\sigma_y = 500$ MPa, $L = 1.25$ mm. The iso-lines indicate the equivalent plastic strain.

In the following, the scaling relations for the maximum $\hat{C}_{inh}$-values shall be discussed. The stress–strain curves of two material points left and right of the interface are depicted schematically in Fig. 10. The strain energy density, ϕ, of Material 1 is given by the area [0–2–4–7–0], those of Material 2 by the area [0–3–5–6–0]. When forming now the integrant of Eq. (2), $[[\phi]] - \boldsymbol{\sigma}[[\boldsymbol{\varepsilon}]]$, it is seen that the area [4–5–6–7–4] cancels and there remains the area [0–2–3–0]. This area can be expressed as $\sigma_y^2 \frac{E_1 - E_2}{2E_1E_2}$. Integrating now this expression along the whole interface of length $2h$ yields a simple estimate for the maximum $\hat{C}_{inh}$-values,

$$\max(\hat{C}_{inh}) \approx \sigma_y^2 \frac{E_1 - E_2}{E_1 E_2} h. \tag{10}$$

According to this estimate, the maximum $\hat{C}_{inh}$-values should not depend on the ligament length, $b = W - a$, although the limit load does. Fig. 11 compares the estimated maximum $\hat{C}_{inh}$-values from Eq. (10) to the values determined by the computations. The agreement is good; the relative error is always less than 10%.

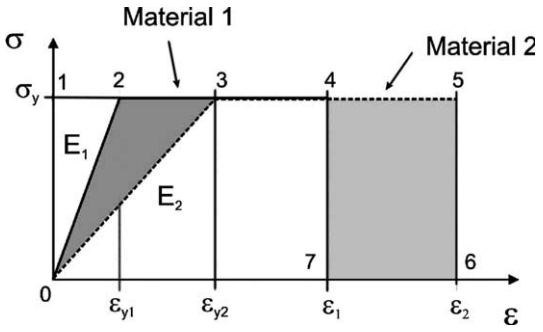

Fig. 10. Schematic stress–strain curves of two material points left and right of the interface for an elastic-ideally plastic bimaterial specimen with constant yield stress and an inhomogeneity in the Young' modulus. The strain energy density of Material 1 is given by the area [0–2–4–7–0], those of Material 2 by the area [0–3–5–6–0]. The material inhomogeneity term is largely influenced by the area [0–2–3–0].

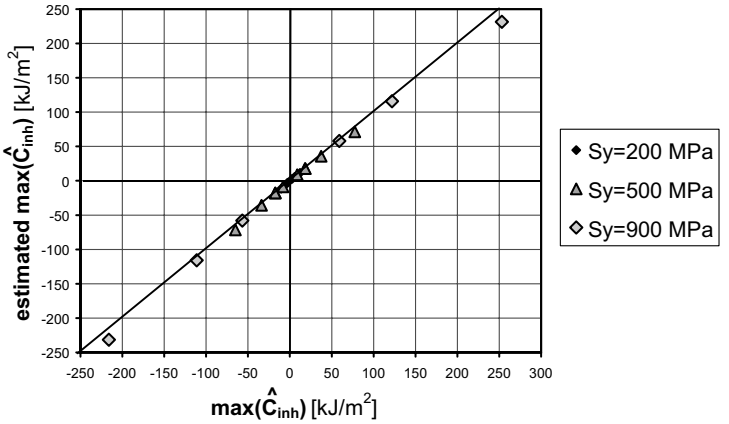

Fig. 11. Estimated maximum saturation values of the material inhomogeneity term, $\max(\hat{C}_{\text{inh}})$, according to Eq. (10) for elastic-ideally plastic bimaterial specimens with constant yield stress and inhomogeneity in the Young' modulus, compared to the values determined via the finite element computations. The relative error is always less than 10%.

4.3. Effect of strain hardening

Up to now, we have considered bimaterial specimens consisting of two non-hardening materials. Now the influence of the strain hardening coefficient on the material inhomogeneity term for bimaterials with a Young's modulus inhomogeneity shall be examined. The computations are made for a Young's modulus of either 210 or 70 GPa, a yield stress $\sigma_y = 500$ MPa, and $L = 0.60$ mm. A power-law hardening material is assumed,

$$\sigma = \sigma_y \left(\frac{\varepsilon}{\varepsilon_y} \right)^N, \tag{11}$$

where ε_y denotes the yield strain, σ_y/E. It is seen in Fig. 12 that the C_{inh}-values do not saturate for $N = 0.1$ and $N = 0.2$. For large loading, C_{inh} increases appreciably due to the hardening, e.g., at $J_{\text{far}} = 380$ kJ/m^2, the value of C_{inh} for $N = 0.2$ is roughly twice that of the non-hardening material. It is interesting that for the compliant/stiff transition the work hardening has only a small influence on C_{inh} until the point where

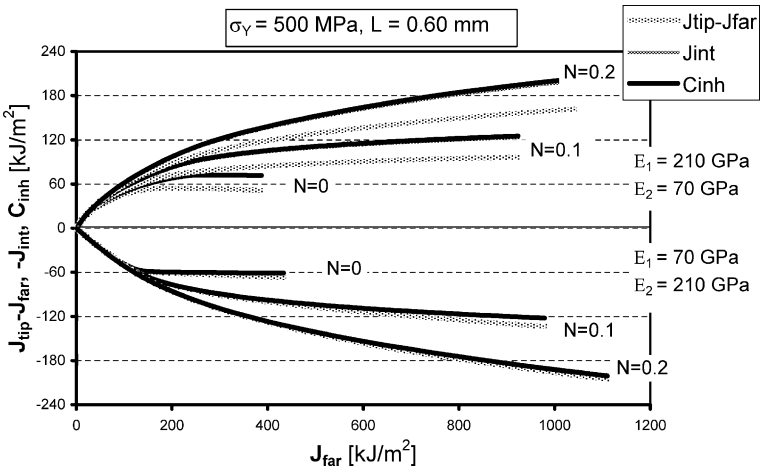

Fig. 12. The effect of the strain hardening on the material inhomogeneity term, C_{inh}, for an elastic-ideally plastic bimaterial specimen with constant yield stress and an inhomogeneity in the Young's modulus (210 and 70 GPa, respectively). N is the exponent of the power-law hardening stress–strain curve.

the non-hardening curve saturates; this is not so for the stiff/compliant transitions. C_{inh} and J_{int} coincide well, but $(J_{\text{tip}} - J_{\text{far}})$ shows some deviation for larger J_{far}-values, especially, for the stiff/compliant transition.

5. Summary

A case study has been presented, exploring how a sharp bimaterial interface perpendicular to the crack plane influences the effective crack driving force in a fracture mechanics specimen. The effect of an inhomogeneity of the elastic modulus, E, in linear elastic and elastic–plastic (non-hardening and hardening) bimaterials under plane strain conditions has been examined. The material properties and the distance between the crack tip and the interface, L, have been systematically varied. The effect of the material inhomogeneity is captured in form of the material inhomogeneity term, C_{inh}. This term can be either evaluated by a simple post-processing procedure following a conventional finite element stress analysis, or by evaluating the J-integral along a contour around the interface, J_{int}. The effective, near-tip crack driving force, J_{tip}, is the sum of C_{inh} and the nominally applied far-field crack driving force, J_{far}.

When a crack approaches the interface to a more compliant material, the material inhomogeneity term, C_{inh}, is positive and J_{tip} becomes larger than J_{far}; a transition into a stiffer material leads to a negative C_{inh}, and J_{tip} becomes smaller than J_{far}. This is so also if the crack has already penetrated the interface.

For linear elastic bimaterials, C_{inh} is proportional to J_{far}, the first Dundurs parameter, $(E_1 - E_2)/(E_1 + E_2)$, and a geometry factor, $\Psi(L,h)$, where h is the half-height of the specimen perpendicular to the crack-plane. When the crack comes close to the interface, C_{inh} can become very large so that, in the limit for $L = 0$, the crack driving force reduces to zero for the compliant/stiff transition; for the stiff/compliant transition, the crack driving force becomes infinite.

For elastic–plastic bimaterials with a constant yield stress, σ_{y}, and zero hardening, C_{inh} first increases with J_{far}, but reaches finally a saturation value, $\hat{C}_{\text{inh}}$. The maximum possible saturation value,$\hat{C}_{\text{inh}}$, which appears when the crack tip is some distance before the interface, scales with σ_{y}^2, $(E_1 - E_2)/(E_1 E_2)$, and h. For a strain hardening material, C_{inh} does not reach a saturation value and may increase appreciably above the $\hat{C}_{\text{inh}}$-value of a comparable non-hardening material.

The results in this paper show that the effective crack driving force, J_{tip}, can be accurately determined as the sum of the material gradient term, C_{inh}, and the nominally applied far-field crack driving force, J_{far}, even in cases where a direct evaluation of J_{tip} does not yield satisfying results.

The effect of the inhomogeneity of the yield stress and the strain hardening exponent, and the simultaneous variation of all the material parameters, will be treated in a separate paper. The strong influence of material inhomogeneities on the crack driving force offers great possibilities for optimizing composite materials and structural components by an intentional variation of the material properties so that the fracture resistance increases. For functionally graded or layered materials some examples are shown in Kolednik (2000).

Acknowledgments

The authors acknowledge gratefully the Materials Center Leoben for funding this work under the project numbers SP7 and SP14. JP thanks the Austrian Exchange Service for partially funding research visits to Leoben under the project number Sl-A 12/0405.

References

Abendroth, M., Groh, U., Kuna, M., Ricoeur, A., 2002. Finite element computation of the electromechanical *J*-integral for 2D and 3D crack analysis. International Journal of Fracture 114, 359–378.

Bahr, H.-A., Balke, H., Fett, T., Hofinger, I., Kirchhoff, G., Munz, D., Neubrand, A., Semenov, A.S., Weiss, H.-J., Yang, Y.Y., 2003. Cracks in functionally graded materials. Materials Science and Engineering A362, 2–16.

Denzer, R., Barth, F.J., Steinmann, P., 2003. Studies in elastic fracture mechanics based on the material force method. International Journal for Numerical Methods in Engineering 58, 1817–1835.

Dundurs, J., 1969. Edge-bonded dissimilar orthogonal elastic wedges. ASME Journal of Applied Mechanics 36, 650–652.

Eshelby, J.D., 1970. Energy relations and the energy–momentum tensor in continuum mechanics. In: Kanninen, M., Adler, W., Rosenfield, A., Jaffee, R. (Eds.), Inelastic Behavior of Solids. McGraw-Hill, New York, pp. 77–115.

Gurtin, M.E., 2000. Configurational Forces as Basic Concepts of Continuum Physics. Springer, Berlin.

Gurtin, M.E., Podio-Guidugli, P., 1996. Configurational forces and the basic laws for crack propagation. Journal of the Mechanics and Physics of Solids 44, 905–927.

Honein, T., Herrmann, G., 1997. Conservation laws in nonhomogeneous plane elastostatics. Journal of the Mechanics and Physics of Solids 45, 789–805.

Jivkov, A.P., Ståhle, P., 2003. A model for graded materials with application to cracks. International Journal of Fracture 124, 93–105.

Kichuchi, M., Miyamoto, H., 1984. Application of the *J* integral concept to microscopic fracture mechanics. In: Carlsson, J., Ohlson, N.G. (Eds.), Mechanical Behavior of Materials IV, Proceedings of the Fourth International Conference, vol. 2. Pergamon, Oxford, UK, pp. 1077–1083.

Kienzler, R., Herrmann, G., 2000. Mechanics in Material Space. Springer, Berlin.

Kim, J.-H., Paulino, G.H., 2003. T-stress, mixed-mode stress intensity factors, and crack initiation angles in functionally graded materials: a unified approach using the interaction integral method. Computer Methods in Applied Mechanics and Engineering 192, 1463–1494.

Kim, A.S., Suresh, S., Shih, C.F., 1997. Plasticity effects on fracture normal to interfaces with homogeneous and graded compositions. International Journal of Solids and Structures 34, 3415–3432.

Kolednik, O., 2000. The yield stress gradient effect in inhomogeneous materials. International Journal of Solids and Structures 37, 781–808.

Kolling, S., Baaser, H., Gross, D., 2002. Material forces due to crack-inclusion interaction. International Journal of Fracture 118, 229–238.

Maugin, G.A., 1993. Material Inhomogeneities in Elasticity. Chapman and Hall, London.

Mueller, R., Maugin, G.A., 2002. On material forces and finite element discretizations. Computational Mechanics 29, 52–60.

Mueller, R., Kolling, S., Gross, D., 2002. On configurational forces in the context of the finite element method. International Journal for Numerical Methods in Engineering 53, 1557–1574.

Pippan, R., Flechsig, K., Riemelmoser, F.O., 2000. Fatigue crack propagation behavior in the vicinity of an interface between materials with different yield stresses. Materials Science and Engineering A283, 225–233.

Rao, B.N., Rahman, S., 2003. Mesh-free analysis of cracks in isotropic functionally graded materials. Engineering Fracture Mechanics 70, 1–27.

Rice, J.R., 1968. A path independent integral and the approximate analysis of strain concentration by notches and cracks. Journal of Applied Mechanics 35, 379–386.

Simha, N.K., 2000. Toughening by phase boundary propagation. Journal of Elasticity 59, 195–211.

Simha, N.K., Shan, G.X., Kolednik, O., Fischer, F.D., 2002. Influence of a bimaterial interface on the crack driving force in elastic and elastic–plastic materials. In: Srivatsan, T.S., Lesuer, D.R., Taleff, E. (Eds.), Modeling of the Performance of Engineering Structural Materials III. The Minerals. Metals & Materials Society, Warrendale, PA, USA, pp. 149–160.

Simha, N.K., Fischer, F.D., Kolednik, O., Chen, C.R., 2003. Inhomogeneity effects on the crack driving force in elastic and elastic–plastic materials. Journal of the Mechanics and Physics of Solids 51, 209–240.

Simha, N.K., Predan, J., Kolednik, O., Fischer, F.D., Shan, G.X. Inhomogeneity effects on the crack driving force in elastic and elastic–plastic materials. Part II: Sharp interfaces. Journal of the Mechanics and Physics of Solids, submitted.

Steinmann, P., 2000. Application of material forces to hyperelastostatic fracture mechanics. Part i: Continuum mechanical setting. International Journal of Solids and Structures 37, 7371–7391.

Steinmann, P., Ackermann, D., Barth, F.J., 2001. Application of material forces to hyperelastostatic fracture mechanics. Part ii: Computational setting. International Journal of Solids and Structures 38, 5509–5526.

Suresh, S., Sugimura, Y., Tschegg, E., 1992. The growth of a fatigue crack approaching a perpendicularly-oriented, bimaterial interface. Scripta Metallurgica 27, 1189–1194.

Suresh, S., Sugimura, Y., Ogawa, T., 1993. Fatigue cracking in materials with brittle surface coatings. Scripta Metallurgica 29, 237–242.

Wang, B.L., Mai, Y.-W., Noda, N., 2003. Fracture mechanics analysis model for functionally graded materials with arbitrarily distributed properties. International Journal of Fracture 116, 161–177.

Weichen, S., 2003. Path-independent integrals and crack extension force for functionally graded materials. International Journal of Fracture 119, L83–L89.